Serine protease activity contributes to control of *Mycobacterium tuberculosis* in hypoxic lung granulomas in mice

Stephen T. Reece,[1] Christoph Loddenkemper,[2] David J. Askew,[3] Ulrike Zedler,[1] Sandra Schommer-Leitner,[1] Maik Stein,[1] Fayaz Ahmad Mir,[1] Anca Dorhoi,[1] Hans-Joachim Mollenkopf,[4] Gary A. Silverman,[3] and Stefan H.E. Kaufmann[1]

[1]Department of Immunology, Max Planck Institute for Infection Biology, Berlin, Germany. [2]Institute for Pathology, Charité — Universitätsmedizin Berlin, Campus Benjamin Franklin, Berlin, Germany. [3]University of Pittsburgh Medical Center Newborn Medicine Program, Children's Hospital of Pittsburgh, and Magee-Womens Hospital, Pittsburgh, Pennsylvania, USA. [4]Core Facility, Max Planck Institute for Infection Biology, Berlin, Germany.

The hallmark of human *Mycobacterium tuberculosis* infection is the presence of lung granulomas. Lung granulomas can have different phenotypes, with caseous necrosis and hypoxia present within these structures during active tuberculosis. Production of NO by the inducible host enzyme NOS2 is a key antimycobacterial defense mechanism that requires oxygen as a substrate; it is therefore likely to perform inefficiently in hypoxic regions of granulomas in which *M. tuberculosis* persists. Here we have used *Nos2*$^{-/-}$ mice to investigate host-protective mechanisms within hypoxic granulomas and identified a role for host serine proteases in hypoxic granulomas in determining outcome of disease. *Nos2*$^{-/-}$ mice reproduced human-like granulomas in the lung when infected with *M. tuberculosis* in the ear dermis. The granulomas were hypoxic and contained large amounts of the serine protease cathepsin G and clade B serine protease inhibitors (serpins). Extrinsic inhibition of serine protease activity in vivo resulted in distorted granuloma structure, extensive hypoxia, and increased bacterial growth in this model. These data suggest that serine protease activity acts as a protective mechanism within hypoxic regions of lung granulomas and present a potential new strategy for the treatment of tuberculosis.

Introduction

Tuberculosis causes significant human mortality and morbidity worldwide, with the lung granuloma representing the typical site of disease manifestation (1, 2). Granulomas are stratified structures, containing concentric layers of T cells and *Mycobacterium tuberculosis*–infected (*M. tuberculosis*–infected) macrophages, which in turn are directed by cytokines, such as IFN-γ and TNF-α, to control bacterial replication. Tuberculosis can be triggered from subclinical latent infection by treatments for inflammatory disorders that block TNF-α (3, 4) or failing $CD4^+$ T cell immunity associated with HIV infection (5). During disease, multiple granuloma phenotypes, including solid nonnecrotizing and caseous necrotic granulomas are present in the lung (6, 7). Events governing granuloma development during tuberculosis remain ill defined. The Ghon complex, a single lesion in the midregion of the lung, together with a single lesion in the hilar lymph node, is a marker for latent infection (8). It has been suggested that break down of the lymphoid component of this complex results in hematogenous dissemination of *M. tuberculosis* to other regions of the lung, in which caseous necrotic granulomas form containing hypoxic regions (9). *M. tuberculosis* persisting within these structures is refractory to most frontline antibiotics, making clinical patient cure lengthy (10), and new drug regimens for tuberculosis treatment should be effective under hypoxic conditions to target these bacilli (11). An understanding of host-protective mechanisms operative within hypoxic granulomas could lead to novel intervention strategies.

Mice infected with *M. tuberculosis* via an aerosol or intravenous route produce granulomas that differ markedly from those seen in humans and fail to reproduce granuloma hypoxia (12–14). In the current work, we show that dissemination of *M. tuberculosis* to the lung from a lymphatic lesion in *Nos2*$^{-/-}$ mice resulted in formation of solid nonnecrotizing granulomas similar to those seen in human tuberculosis. Temporary blocking of IFN-γ or TNF-α in vivo resulted in development of granuloma pathology characterized by increased numbers of granulomas demonstrating hypoxia, caseation, and exacerbated growth of *M. tuberculosis*. We exploited this model further to attribute a critical role for host serine proteases in the control of *M. tuberculosis* in hypoxic regions of granulomas. Thus, we present an experimental window on early events in development of hypoxic caseous granulomas during active tuberculosis and highlight a molecular mechanism that plays a critical role in determining its pathological outcome.

Results

Dermal infection of Nos2$^{-/-}$ *mice produces a Ghon complex-like structure from which M. tuberculosis disseminates to the lung in which human-like granulomas develop*. Although tuberculosis today is primarily a pulmonary disease, cutaneous tuberculosis (lupus vulgaris) in humans occurs via primary inoculation of *M. tuberculosis* in the dermis, in which an ulcerated lesion develops in the skin, accompanied by a necrotic lesion in the corresponding lymph node (15). Since these lesions typically heal without systemic dissemination of *M. tuberculosis* via the lymphatic system, this structure is considered analogous to the pulmonary Ghon complex (16). We investigated whether *M. tuberculosis* infection of the ear dermis in mice results in formation of a similar structure. The production of NO via the enzyme NOS2 in response to IFN-γ signalling is a key protective mechanism against *M. tuberculosis* (17), and WT and *Nos2*$^{-/-}$ mice are radically different in their ability to control

Conflict of interest: The authors have declared that no conflict of interest exists.
Citation for this article: *J Clin Invest.* 2010;120(9):3365–3376. doi:10.1172/JCI42796.

primary *M. tuberculosis* infection. After pulmonary *M. tuberculosis* infection via aerosol, WT mice can survive a chronic pulmonary infection of approximately 10^6 CFUs per lung for approximately 200 days (12). Similarly, infected *Nos2*$^{-/-}$ mice succumb to infection after approximately 40 days (18, 19). To investigate the outcome on primary dermal challenge, C57BL/6 WT and *Nos2*$^{-/-}$ mice were infected with 10^4 *M. tuberculosis* in the ear dermis, and growth of *M. tuberculosis* in the ear dermis, the dermis draining auricular lymph node (dLN), and spleen was evaluated (Supplemental Figure 1A; supplemental material available online with this article; doi:10.1172/JCI42796DS1). Both mouse strains demonstrated an initial replication of *M. tuberculosis* in dermis as well as lymph node for 2 weeks. From day 14 to 56 after infection (p.i.), WT mice controlled *M. tuberculosis* growth in the dermis and dLN in the absence of marked pathology. *Nos2*$^{-/-}$ mice developed a dermal lesion that ulcerated by day 56 p.i. and a necrotic lesion with infiltrates of neutrophils and macrophages in the draining lymph node on days 28 and 56 p.i. (Supplemental Figure 1, B and C). These pathologies were accompanied by an inability to reduce *M. tuberculosis* replication at either site. Dissemination of *M. tuberculosis* from the dLN via hematogenous spread occurred as evidenced by stable *M. tuberculosis* infection of the spleen (Supplemental Figure 1A) and the lung. Replication of *M. tuberculosis* stabilized in the lungs of *Nos2*$^{-/-}$ mice between days 28 and 56 p.i., while lungs of WT mice remained clear of cultivable *M. tuberculosis* (Supplemental Figure 2). We compared growth of *M. tuberculosis* in the lungs of *Nos2*$^{-/-}$ mice infected with aerosol and dermal routes. Aerosol-infected mice demonstrated the typical pattern of *M. tuberculosis* growth in the lung, peaking at approximately day 30 p.i., shortly after which *Nos2*$^{-/-}$ mice succumbed. Strikingly, exponential growth of *M. tuberculosis* in the lung was prevented in dermal-infected *Nos2*$^{-/-}$ mice (Figure 1A). Nonnecrotizing granulomas developed in lungs of *Nos2*$^{-/-}$ mice by day 28 p.i. and were still present at day 56 p.i. These structures were undetectable in WT mice and distinct from lesions typically observed in the mouse lung after aerosol infection (20, 21), demonstrating configurations of T cells and macrophages as found in the classic stratified nonnecrotizing human granuloma observed during active tuberculosis (Figure 1B). We compared the *M. tuberculosis*–specific T cell response generated in the lung after dermal and aerosol infection in WT and *Nos2*$^{-/-}$ mice by measuring TNF-α and IFN-γ production by pulmonary CD4$^+$ T cells in response to the dominant *M. tuberculosis* antigen ESAT-6. At day 14 p.i., numbers of T cells in the lungs of dermal-infected *Nos2*$^{-/-}$ mice producing both TNF-α and IFN-γ in response to ESAT-6 were significantly higher than those in aerosol-infected *Nos2*$^{-/-}$ mice (Figure 1C and Supplemental Figures 3 and 4). By day 28 p.i., numbers of CD4$^+$ T cells producing both TNF-α and IFN-γ were comparable in both aerosol- and dermal-infected mice. Therefore, dermal-infected *Nos2*$^{-/-}$ mice demonstrated earlier ESAT-6–specific CD4$^+$ T cell responses in the lung in the face of significantly lower CFUs compared with aerosol-infected mice (Figure 1A).

In vivo blocking of IFN-γ or TNF-α in dermal-infected Nos2$^{-/-}$ *mice results in development of classic human granuloma pathology*. We next investigated whether blocking of TNF-α and IFN-γ in vivo would impact granuloma formation and disease progression in the lungs of dermal-infected *Nos2*$^{-/-}$ mice. Cytokines were blocked by intraperitoneal administration of specific mAb on days 14 and 21 p.i. Mice suffered 10-fold higher bacterial load at day 28 p.i. after blocking of TNF-α or IFN-γ and up to 100-fold higher load at day 56 p.i. in the lung compared with control mice (Figure 1D). After IFN-γ blocking, mice demonstrated significantly lower CD4$^+$ T cell frequencies in the lung producing TNF-α and IFN-γ in response to ESAT-6 or purified protein derivative (PPD) at day 28 p.i. compared with those of TNF-α–blocked mice (Supplemental Figure 5). At day 56 p.i., blocking of either TNF-α or IFN-γ caused an increase in numbers of granulomas in the lung compared with control mice, with a proportion demonstrating central caseous necrotic regions (Figure 2A). Acid-fast *M. tuberculosis* was stained in central necrotic areas of caseous granulomas containing scant host cells and in the cellular area encircling the necrotic region (Figure 2B). Necrotic areas in granulomas were clearly demarcated by stratified T cells and macrophages that reflected the spatial organization of T cells and macrophages in human caseous granulomas during active tuberculosis (Supplemental Figure 6A). We sectioned the entire left lobe of the lung and enumerated numbers of nonnecrotizing and caseous granulomas. Both total numbers of granulomas and numbers of caseous granulomas were significantly increased in cytokine-blocked mice compared with those of controls (Figure 2C). We occasionally detected a single caseous granuloma in control mice, demonstrating that IFN-γ and TNF-α blocking in this model is not essential for granuloma caseation. Despite this, percentages of enumerated granulomas demonstrating caseous necrosis significantly increased after IFN-γ and TNF-α blocking, indicating that granuloma caseation is exacerbated by immune suppression (Figure 2D). T cells and macrophages are the predominant cell types seen in human granulomas (22), contrasting with neutrophilic infiltrates predominantly seen in granulomatous lesions of *Nos2*$^{-/-}$ mice after aerosol infection (21, 23). To further qualify our assertion that caseous granulomas observed after dermal infection of *Nos2*$^{-/-}$ mice were more representative of human granulomas, we stained lungs of aerosol-infected mice at day 30 p.i. and IFN-γ– or TNF-α–blocked dermal-infected mice at day 56 p.i. for the major neutrophil product myeloperoxidase (MPO). Granulomatous lesions in aerosol-infected mice stained strongly for MPO, while caseous granulomas after dermal infection showed markedly lower levels of MPO (Supplemental Figure 7), adding an additional layer of evidence in support of them being more representative of those in human tuberculosis. Development of caseous granulomas does not typically occur during experimental tuberculosis of mice (24). Recent studies suggest that products of the *sst1* genetic locus in mice prevent development of necrotic lung lesions during murine tuberculosis (25, 26). Caseous granulomas formed during *M. tuberculosis* infection of guinea pigs, rabbits, and nonhuman primates demonstrate hypoxic cells in regions proximal to the central necrotic zone (14). Despite similarities in these pathologies, only low-dose infection of nonhuman primates resulted in tuberculosis that reactivated from a latent stage and convincingly reproduced the spectrum of granulomatous lesions at a low bacterial load characteristic of human tuberculosis (27, 28). This suggests that there are inconsistencies in how hypoxic granulomas are reproduced in these models. To further evaluate the relevance of our model to the human disease, granuloma hypoxia was assessed using pimonidazole hydrochloride (PIMO), an in vivo hypoxia marker used in both humans and animal models (13, 14, 29–31). At low O_2 partial pressure in tissue, PIMO enters cells, becomes activated by host nitroreductases, and binds protein thiol groups to form adducts detectable using immunohistology in tissue sections. Infected mice, with or without IFN-γ or TNF-α blocking, were treated with PIMO (50 mg/kg) at day 56 p.i., sacrificed 2 hours later, and lung sections were investigated for

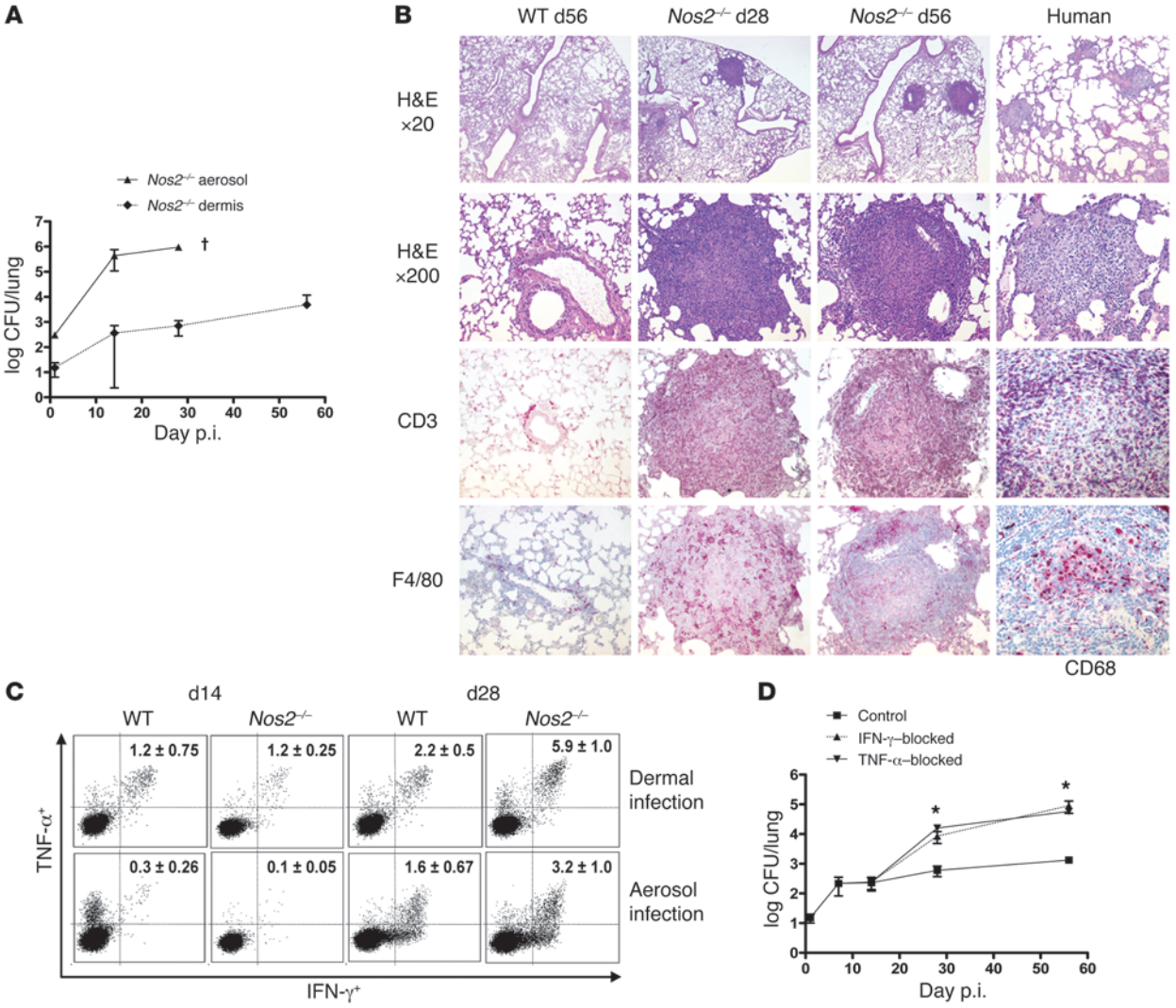

Figure 1

Nonnecrotizing granulomas form in lungs of dermal-infected *Nos2*$^{-/-}$ mice that require TNF-α or IFN-γ to prevent growth of *M. tuberculosis*. (**A**) Comparison of *M. tuberculosis* growth in lungs of aerosol-infected or dermal-infected *Nos2*$^{-/-}$ mice. CFUs from homogenates were enumerated on days 1, 14, 28, and 56 p.i. (mean ± SEM; $n = 5$). The "†" indicates the time point at which aerosol-infected *Nos2*$^{-/-}$ mice succumb to infection. (**B**) H&E staining of *Nos2*$^{-/-}$ lung tissue at days 28 and 56 p.i. demonstrated presence of nonnecrotizing granulomas that were undetectable in WT mice at day 56 (original magnification, ×20). Nonnecrotizing granulomas in *Nos2*$^{-/-}$ lungs stained positively with anti-CD3 and anti-F4/80 mAbs, demonstrating presence of T cells and macrophages, respectively. These structures resembled nonnecrotizing granulomas observed during active human tuberculosis stained for T cells and macrophages with anti-CD3 and anti-CD68, respectively. (**C**) Cells purified from lungs of infected mice at days 14 and 28 p.i. were stimulated for 6 hours with ESAT-6 peptide, stained for surface CD4, intracellular IFN-γ, and TNF-α, and analyzed by FACS. Panels show cells purified from mice after dermal or aerosol infection. Numbers show percentages of CD4$^+$ IFN-γ$^+$ TNF-α$^+$ cells out of total CD4$^+$-gated T cells ± SEM ($n = 3$). Despite reduced bacterial load compared with aerosol-infected mice, dermal-infected mice prime robust CD4$^+$ T cell responses against ESAT-6 that were detectable in the lung by day 14 p.i. (**D**) Lung CFUs from TNF-α– or IFN-γ–blocked and control *Nos2*$^{-/-}$ mice at days 1–56 p.i. (mean ± SEM; $n = 5$). TNF-α– or IFN-γ–blocked *Nos2*$^{-/-}$ mice at days 28 and 56 p.i. had significantly elevated CFUs compared with control mice. *$P < 0.05$.

the presence of PIMO adducts. We could reliably identify hypoxic regions in all caseating granulomas (Figure 3A). Strong staining of PIMO adducts was observed in cells encircling the necrotic region in all caseous granulomas analyzed, as observed in other animal models demonstrating granuloma hypoxia during tuberculosis (13, 14). Taken together, these data suggest that in our model the extent of hypoxia within granulomas increases after immunosuppression (Figure 3B) and is associated with necrotic regions in caseous granulomas.

The serine protease cathepsin G is abundant in hypoxic regions of granulomas. We next attempted to identify potential molecular markers of development of granuloma caseation and hypoxia during tuberculosis. TNF-α–blocked mice lacked defined granuloma structures in the lung at day 28 p.i., while IFN-γ–blocked mice demonstrated granulomas with central caseous necrosis at day 28 p.i. (approximately 1 out of 5 sections analyzed). mRNA transcripts from lungs were compared by competitive microarrays among WT, *Nos2*$^{-/-}$, and IFN-γ–blocked *Nos2*$^{-/-}$ mice at day 28 p.i. Transcripts

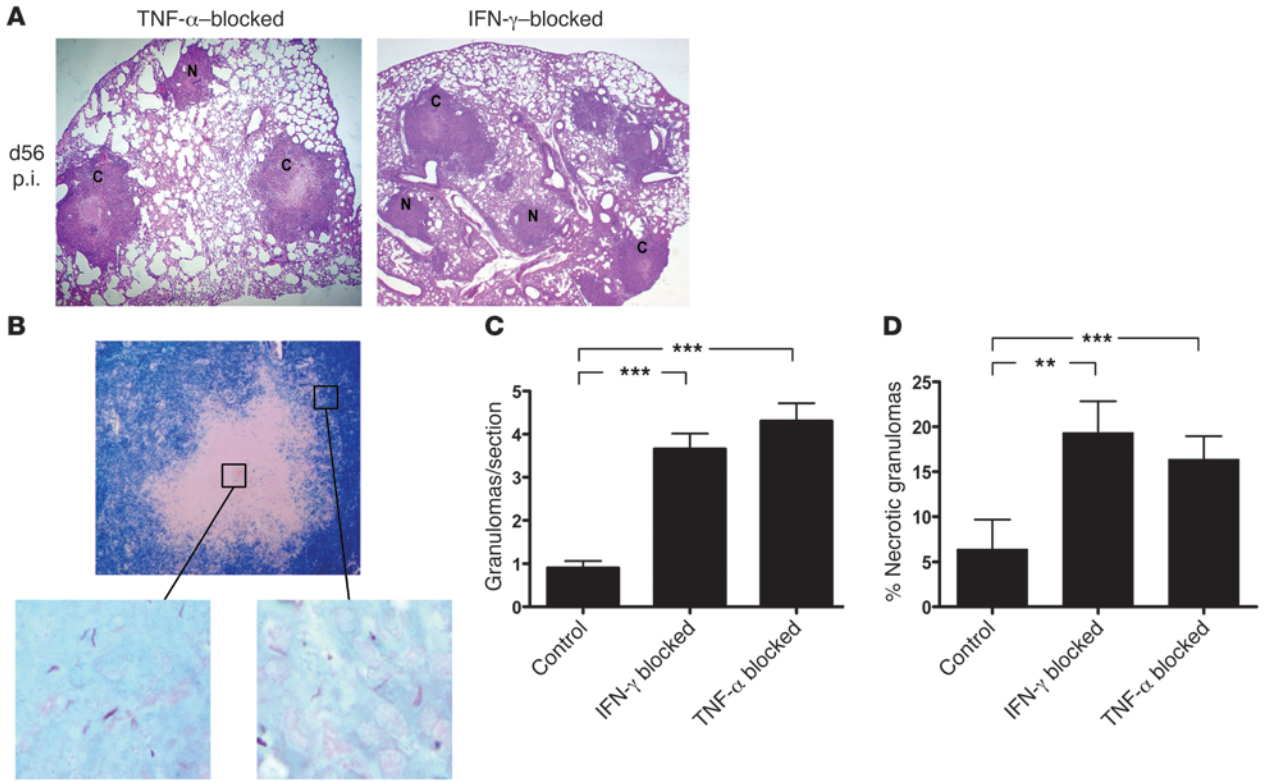

Figure 2

Blocking of TNF-α or IFN-γ leads to development of caseous necrosis within granulomas. (**A**) H&E staining of lung tissue at day 56 p.i. demonstrated the presence of nonnecrotizing (N) and caseous granulomas (C), after blocking of TNF-α or IFN-γ in *Nos2*$^{-/-}$ mice (original magnification, ×25). (**B**) Giemsa staining of caseous granulomas distinguished the central necrotic region from the cellular periphery (original magnification, ×200). Ziehl-Neelsen staining revealed presence of *M. tuberculosis* in both locations. Regions within the rectangles are shown at higher magnification (original magnification, ×1,000). (**C**) Number of granulomas per section in control mice and after blocking of TNF-α or IFN-γ. The entire left lobe was sectioned, H&E stained, and the total number of granulomas per section were enumerated per mouse (n = 5). Blocking of TNF-α or IFN-γ caused significantly increased numbers of granulomas per section and (**D**) significantly increased percentages of granulomas demonstrating caseous necrosis per section compared with control mice (mean ± SEM; n = 5). $^{**}P < 0.01$; $^{***}P < 0.001$.

encoding 3 serine proteases, neutrophil elastase (NE), proteinase-3 (Prtn3), and cathepsin G (Ctsg), were upregulated in *Nos2*$^{-/-}$ versus WT mice and further upregulated in IFN-γ–blocked *Nos2*$^{-/-}$ mice (Supplemental Figure 6B). These serine proteases show broad-spectrum antimicrobial activity (32, 33), with expression normally associated with azurophil granules of neutrophils (34) but also detected in macrophages (35–37). Using quantitative RT-PCR (qRT-PCR), we confirmed upregulation of *Ctsg* in the lungs of *Nos2*$^{-/-}$ mice compared with WT mice and further upregulation in IFN-γ–blocked *Nos2*$^{-/-}$ mice at day 28 p.i. (Figure 3C). The Ctsg protein was stained within nonnecrotizing granulomas in the lungs of *Nos2*$^{-/-}$ mice at day 56 p.i. Expression was associated with macrophages and staining was absent in the lungs of WT mice at the equivalent time point (Figure 3D). In granulomas of IFN-γ–blocked *Nos2*$^{-/-}$ mice, Ctsg expression focused on macrophages and granulocytes in the region encircling the central caseous zone, colocalizing with the region that we demonstrated as hypoxic (Figure 3, A and D). Murine Ctsg and human CTSG are highly related in sequence and function (38). Caseous necrotic granulomas in humans demonstrated analogous patterns of CTSG staining, with expression restricted to actively caseating granulomas, because end-stage cavities were devoid of CTSG staining (Figure 4A). NO production is likely abrogated in hypoxic regions of granulomas, since NOS2 requires O_2 for its synthesis (39, 40). In addition, unregulated serine protease activity in the lung can exacerbate cellular stress during inflammation (41–43). Therefore, activated *M. tuberculosis*–infected macrophages in hypoxic areas of granulomas are potentially subjected to serine protease-induced cellular stress and are deprived of a major antimycobacterial defence mechanism, which could contribute to the development of granuloma pathology. We investigated whether addition of Ctsg to *M. tuberculosis*–infected activated bone marrow–derived macrophages (BMDMs) induced cellular stress that impacted both necrosis and growth of *M. tuberculosis*. Addition of CTSG to culture media had no effect on necrosis of uninfected activated macrophages, as measured by lactate dehydrogenase (LDH) activity in culture supernatants. After 72 hours of *M. tuberculosis* infection, CTSG enhanced necrosis of activated *Nos2*$^{-/-}$ macrophages but not WT macrophages (Figure 4B). Macrophage necrosis was also enhanced by addition of CTSG to activated WT macrophages after inhibition of NO production (Figure 4B). Enhanced necrosis of activated *Nos2*$^{-/-}$ BMDMs by CTSG was not recapitulated by addition of exogenous NE (Figure 4C), while both exogenous CTSG and NE significantly decreased bacterial proliferation measured at 72 hours p.i. (Figure 4D). We confirmed reduced bacterial growth in activated *Nos2*$^{-/-}$ BMDMs after addition of CTSG

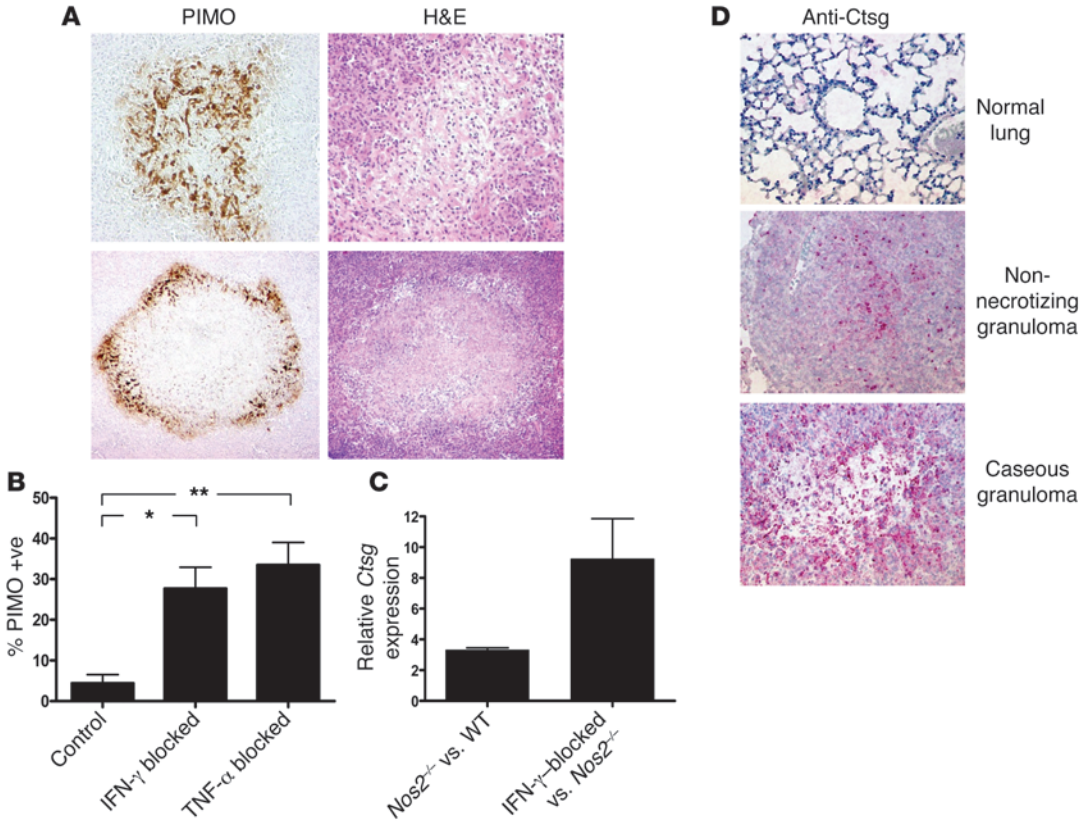

Figure 3

Hypoxia and Ctsg expression is associated with granuloma pathology. (**A**) Dermal-infected mice (day 56 p.i.), with and without blocking of TNF-α or IFN-γ, received the tissue hypoxia marker PIMO ($n = 5$) and were sacrificed 2 hours later, and lung sections were stained for the presence of PIMO adducts. One hundred percent of caseous necrotic granulomas in all groups stained positive for PIMO adducts. Images show typical PIMO staining in granulomas after cytokine blocking (original magnification, ×100 [top]; ×200 [bottom]). (**B**) Numbers of PIMO-positive granulomas (PIMO +ve) were significantly higher after blocking of TNF-α or IFN-γ (mean ± SEM; $n = 5$). (**C**) Relative mRNA expression of *Ctsg* in individual *Nos2*$^{-/-}$ versus WT mice and IFN-γ–depleted *Nos2*$^{-/-}$ versus untreated *Nos2*$^{-/-}$ mice at day 28 p.i., measured by qRT-PCR on transcribed cDNA and normalized to expression of GAPDH (mean ± SEM; $n = 5$). (**D**) Staining of lung tissue from dermal-infected WT (normal lung), *Nos2*$^{-/-}$ (non-necrotizing), and IFN-γ–depleted *Nos2*$^{-/-}$ (caseous granuloma) mice with anti-Ctsg mAbs at day 56 p.i. (original magnification, ×200). Staining shows cells within nonnecrotizing granulomas expressing Ctsg in *Nos2*$^{-/-}$ mice. Ctsg was detected in regions encircling the central necrotic regions of caseous granulomas in IFN-γ–depleted *Nos2*$^{-/-}$ mice that were identified as hypoxic (Figure 3A). $^{*}P < 0.05$; $^{**}P < 0.01$.

through direct enumeration of CFUs from cell lysates on 7H11 culture plates (Supplemental Figure 8A). These data indicate that, in conditions of low or absent NO production, exogenous CTSG controls intracellular growth of *M. tuberculosis* in vitro at the expense of inducing cellular stress that culminates in necrotic cell death of activated macrophages.

Serpinb3a protects M. tuberculosis–infected macrophages from exuberant serine protease activity. As well as upregulation of serine proteases, IFN-γ blocking also led to a later marked increase in transcripts encoding clade B serine protease inhibitors (serpins) in the lungs of *Nos2*$^{-/-}$ mice (Table 1). These molecules function as intracellular inhibitors of cysteine and serine proteases with distinct cross-class specificity, protecting cells from aberrant proteolysis by a general mechanism, using a C-terminal reactive site loop as bait and acting as a suicide substrate (44, 45). Among these is *Serpinb3a*, the product of which specifically inhibits Ctsg (46, 47) and which, along with *Serpinb3b* and *Serpinb3c*, forms part of the SCCA locus in mice (referred to herein as *serpinb3a/b/c*) (48). Using qRT-PCR, we confirmed upregulation of *serpinb3a/b/c* in the lungs of IFN-γ–blocked *Nos2*$^{-/-}$ mice compared with control mice at day 28 p.i. (Figure 5B). In caseous granulomas of IFN-γ–blocked *Nos2*$^{-/-}$ mice, serpinb3a/b/c expression localized to a region encircling the necrotic area, with expression focused on hypoxic areas that stained similarly for Ctsg (Figure 3, A and D, and Figure 5A). Since Ctsg expression within granulomas morphologically associated with macrophages, we determined whether *serpinb3a/b/c* and *Ctsg* were also upregulated by macrophages during in vitro *M. tuberculosis* infection. After 72 hours of infection, IFN-γ–activated WT and *Nos2*$^{-/-}$ BMDMs showed robust upregulation of *serpinb3a/b/c* and *Ctsg*, while nonactivated, infected BMDMs showed modest downregulation of both genes (Figure 5C). To evaluate the effect of specific inhibition of Ctsg by Serpinb3a in *M. tuberculosis*–infected macrophages, we infected activated WT and *Serpinb3a*$^{-/-}$ BMDMs and measured effects on cell death and *M. tuberculosis* growth in both presence and absence of NO production. When NO production was inhibited in activated macrophages, cell death was significantly enhanced in *M. tuberculosis*–infected *Serpinb3a*$^{-/-}$ BMDMs, despite no differ-

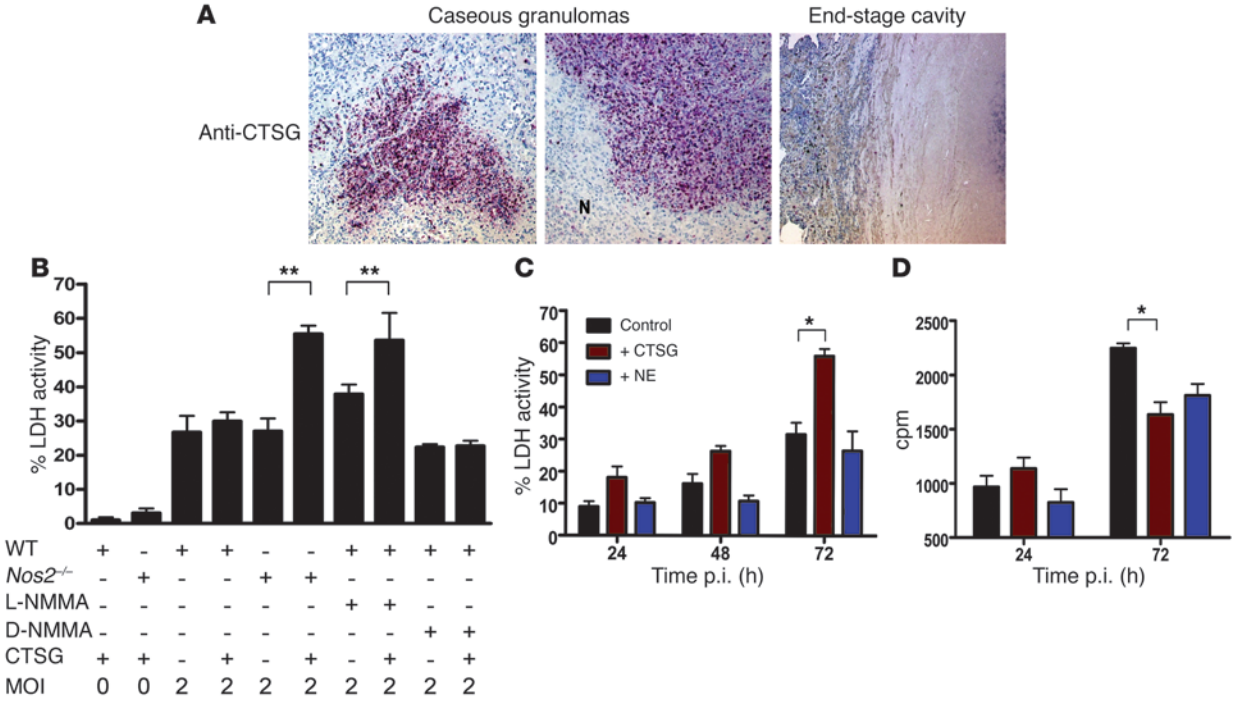

Figure 4

Exogenous CTSG enhances cell death of IFN-γ–activated *M. tuberculosis*–infected macrophages, while controlling intracellular *M. tuberculosis* growth in vitro when NO production is abrogated. (**A**) Lung tissue sections derived from individuals diagnosed with active pulmonary tuberculosis ($n = 6$). Macrophages and granulocytes expressing CTSG, as detected by immunohistochemical staining (original magnification, ×200), localized to the central necrotic region ($n = 3$). Expression of CTSG was not evident within end-stage cavities in human tissues, indicating expression is consistent with active caseation in human granulomas ($n = 3$). (**B**) Level of necrosis of IFN-γ–activated WT or *Nos2*$^{-/-}$ BMDMs, cultured in vitro in the presence of exogenous CTSG. Cell death was measured as the percentage lactase dehydrogenase (LDH) activity in cell supernatants at 72 hours p.i. (MOI 0 or 2). NO production was abrogated in activated macrophages by addition of the competitive inhibitor of NOS2 L-NMMA, with the nonactive isomer D-NMMA as a control. Percentage LDH activity is shown as mean ± SD ($n = 6$). (**C**) Percentage LDH activity in cell supernatants and (**D**) [3H] uracil incorporation (MOI 2) of IFN-γ–activated *Nos2*$^{-/-}$ BMDMs, cultured in vitro in the presence of exogenous CTSG or NE (mean ± SD; $n = 4$). $^{*}P < 0.05$; $^{**}P < 0.01$.

ence in ability to control *M. tuberculosis* replication (Figure 5D). These in vitro data indicate that intracellular regulation of endogenous Ctsg serine protease activity by Serpinb3a prevents death of *M. tuberculosis*–infected macrophages.

Extrinsic serine protease inhibition during granuloma development exacerbates tuberculosis. Since both exogenous Ctsg and a lack of endogenous inhibition of Ctsg serine protease activity similarly enhanced *M. tuberculosis*–infected macrophage cell death, we next asked whether extrinsic serine protease inhibition in vivo led to exacerbation or abatement of tuberculosis, focused on development of granuloma pathology in our model. 4-(2-aminoethyl)-benzenesulphonyl fluoride (AEBSF) is a specific nonreversible inhibitor of serine proteases, suitable for in vivo use (49). Dermal-infected *Nos2*$^{-/-}$ mice were subjected to temporary IFN-γ blocking to induce granuloma pathology and treated with AEBSF twice weekly between day 28 and 56 p.i. By day 56 p.i., AEBSF-treated mice demonstrated significantly elevated levels of CFUs in the lungs compared with those of controls (Figure 6A) This effect specifically localized to the lungs, as bacterial loads in the dLN and spleen were unaffected by administration of this inhibitor (Figure 6A). To verify the efficacy of AEBSF in the lung during tuberculosis, proteins in lung lysates were assayed for their ability to cleave the chromogenic peptide N-succinyl-Ala-Ala-Pro-Phe-P-Nitroanilide (suc-AAPF-pNA). Cleavage of this peptide by Ctsg and other chymotrypsin-like serine proteases produces a color reaction that can be followed by absorbance spectroscopy. This system can be used to measure maximum velocity (Vmax) of CTSG activity, which correlates with enzyme concentration (Supplemental Figure 8C). Vmax of chymotrypsin-like serine protease activity in lung lysates at day 56 p.i. was significantly lower in AEBSF-treated mice versus control mice (Figure 6B), showing a reduction of 30%–40% in enzyme activity. These data indicate partially effective inhibition of Ctsg by AEBSF in the lung during tuberculosis. Differences in pathology in the lungs of AEBSF-treated versus -untreated mice focused on necrotic granulomas, with a general loss of structural integrity at the interface between necrotic and cellular areas in inhibitor-treated mice (Figure 6C). Staining of *M. tuberculosis* within these regions also demonstrated larger numbers of bacteria encircling the necrotic zone in AEBSF-treated mice (Figure 6C). Lesions stained for PIMO adducts revealed marked distortion of hypoxic regions in inhibitor-treated mice compared with those seen in controls (Figure 6D). Dermal-infected *Nos2*$^{-/-}$ mice, which were not treated with IFN-γ blocking antibody, did not develop caseous granulomas in the lung and showed no increase in CFUs in the lung or any other organ after identical AEBSF treatment (Supplemental Figure 8B). We therefore attribute elevation of CFUs in the lung after AEBSF treatment to an inability to limit bacterial growth in hypoxic areas of granulomas.

Table 1
Gene expression of *Nos2*$^{-/-}$ versus WT or IFN-γ–blocked *Nos2*$^{-/-}$ versus control *Nos2*$^{-/-}$ mice

Clade B serpin–encoding gene	*Nos2*$^{-/-}$ vs. WT	IFN-γ–blocked *Nos2*$^{-/-}$ vs. *Nos2*$^{-/-}$
Serpinb1a	–1.01	1.88
Serpinb1b	1.12	1.6
Serpinb1c	1.11	1.78
Serpinb2	**3.78**	1.16
Serpinb3a	**–3.08**	**34.58**
Serpinb3b	**–9.9**	**24.93**
Serpinb3c	**–4.6**	**35.11**
Serpinb5	**–2.6**	**5.44**
Serpinb7	–1.06	**3.8**
Serpinb11	**–3.8**	**20.3**
Serpinb12	**–3.61**	**24.2**
Serpinb13	1.0	**5.42**

Selected results for clade B serpins from competitive microarray analyses of cDNA transcribed from pooled mRNA purified from lungs of mice (n = 3) at day 28 p.i. Numbers are representative of fold change in gene expression of *Nos2*$^{-/-}$ versus WT or IFN-γ–blocked *Nos2*$^{-/-}$ versus control *Nos2*$^{-/-}$ mice. Values where fold changes were more than 2 and P values were less than 0.01 are shown in bold.

Discussion

Here we exploit a model of murine tuberculosis that we believe to be novel, allowing temporal analysis of human-like granuloma pathology. Although this model involves removal of NO production from the macrophage's arsenal of weapons against *M. tuberculosis*, we do not discount a role for NO during human tuberculosis. We do, however, demonstrate circumstances in which granulomas with the canonical properties of those seen in patients with pulmonary tuberculosis develop in the lung in an absence of NO production by activated macrophages infected with *M. tuberculosis*.

Among the classic hallmarks of human granulomas observed in this model are central caseous necrosis and hypoxia, which to our knowledge have not previously been demonstrated in experimental tuberculosis of mice. Because NOS2 requires oxygen as a substrate, it is likely that NO production in hypoxic regions of human granulomas is abrogated. A new tuberculosis drug candidate, PA-824, functions in anaerobic conditions by using a bacterial enzyme to drive nitrite and NO synthesis to kill *M. tuberculosis* and has been mooted as a potential therapy to augment faltering NOS2 efficiency in hypoxic granulomas (40, 50). Our system offers a convenient small animal model for analyzing drugs of this type.

We demonstrated upregulation of the serine proteases Ctsg, NE, and Prtn3 in lung tissue in which caseous hypoxic granulomas formed and detected Ctsg in cells surrounding regions of caseous necrosis in both human and mouse granulomas. Exogenous CTSG but not NE specifically induced cell death of activated *M. tuberculosis*–infected macrophages, while both controlled growth of intracellular *M. tuberculosis*. The substrate specificity of Ctsg and NE are distinct. Ctsg cleaves the C terminus of aromatic or positively charged residues, while NE cleaves the C terminus of small hydrophobic residues (51). Enhanced necrosis in infected macrophages mediated by Ctsg could therefore result from proteolysis of specific target sequences that remain as yet undetermined. We show that Serpinb3a inhibition of Ctsg is required to prevent necrotic cell death of *M. tuberculosis*–infected macrophages activated by IFN-γ. Ctsg, NE, and prtn3 all show antimicrobial activity independently from proteolytic activity (52) and N-terminal cationic peptides deriving from Ctsg have demonstrated ability to reduce *M. tuberculosis* growth in vitro (37). Therefore, specific neutralization of Ctsg by Serpinb3a does not completely abrogate antimicrobial activity. Ctsg was upregulated in the lungs of *Nos2*$^{-/-}$ mice but not WT mice between days 14 and 30 after aerosol *M. tuberculosis* infection and accompanied by a moderate downregulation of serpinb3a/b/c (53). Expression of Ctsg may represent a signature response of activated *Nos2*$^{-/-}$ macrophages to *M. tuberculosis* infection. The strength of our model lies in an ability to reactivate tuberculosis in the lung by blocking IFN-γ and to demonstrate upregulation of Ctsg and serpinb3a/b/c in hypoxic regions of caseous granulomas that do not develop after aerosol infection of mice.

Extrinsic inhibition of serine protease activity by AEBSF enhanced disease progression in the lungs of mice in which hypoxic caseous granulomas developed. Increased pathology and bacterial growth focused on hypoxic regions of granulomas. *M. tuberculosis* replication is probably retarded in hypoxic tissue compared with tissue where oxygen bioavailability is unlimited (54) and differences in CFUs, between treated and untreated mice, were modest. Moreover, inhibition of serine protease activity in the lung on AEBSF treatment was significant but incomplete and more complete inhibition could lead to even more pronounced effects on tuberculosis. AEBSF affects both the neutrophil respiratory burst via inhibition of NADPH oxidase (55) and activity of phospholipase D (56). Phospholipase D increases phagolysosome maturation in *M. tuberculosis*–infected monocytes (57) and although NADPH oxidase deficiency shows no effect on progression of tuberculosis after aerosol infection in mice (21), we cannot discount potential inhibitory effects of these molecules on the development of tuberculosis after dermal infection in our model. However, AEBSF treatment produced effects on tuberculosis exclusively in lung tissue containing significant numbers of hypoxic caseous granulomas in which Ctsg, NE, and prtn3 are the major serine proteases upregulated. Although we cannot completely discount effects of AEBSF on other serine protease-controlled pathways, we conclude that the partial inhibition of these molecules likely contributes to the exacerbation of tuberculosis seen in this study.

We provide evidence that serine protease activity is required for containment of infection in caseous granulomas in which NO production is abrogated, and it will be important to unravel the precise molecular mechanisms by which this protection is achieved. Regulation of serine protease-induced cell death by clade B serpins in *M. tuberculosis*–infected macrophages could serve the host by keeping granulomas intact, while deploying serine protease-mediated control of bacterial growth. We propose that serine proteases are important molecular players in development of tuberculosis focused on hypoxic regions of granulomas. If *M. tuberculosis* proliferates in these regions, necrotic tissue within granulomas eventually liquefies and cavity formation and disease transmission ensues (58). On the other hand, if growth of *M. tuberculosis* is contained, granuloma pathology is arrested, eventually resulting in caseum mineralization and granuloma calcification. Fine tuning of host serine protease activity could represent an attractive strategy for interventions that specifically target this key battleground between host and microbe.

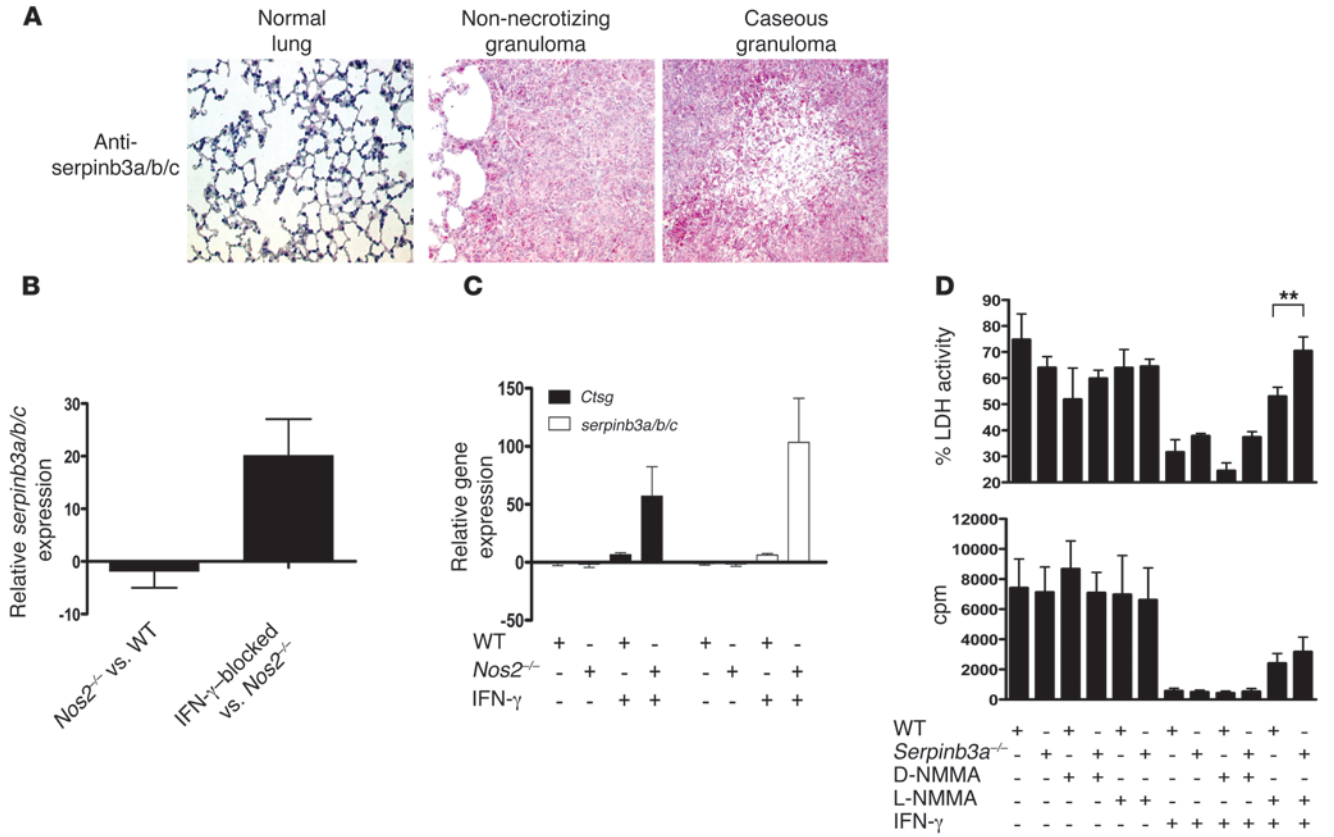

Figure 5

Clade B serpins are expressed in hypoxic regions of caseating granulomas, and endogenous Serpinb3a limits death of activated *M. tuberculosis*–infected macrophages. (**A**) Staining of lungs from dermal-infected WT (normal lung), *Nos2*$^{-/-}$ (nonnecrotizing granulomas), and IFN-γ–depleted *Nos2*$^{-/-}$ (caseous granuloma) mice with anti-Serpinb3a mAbs at day 56 p.i. (original magnification, ×200). serpinb3a/b/c was detected in regions encircling the central necrotic region of caseous granulomas in IFN-γ–depleted *Nos2*$^{-/-}$ mice. (**B**) Relative mRNA expression of *serpinb3a/b/c* in individual IFN-γ–depleted *Nos2*$^{-/-}$ versus untreated *Nos2*$^{-/-}$ mice at day 28 p.i. measured by qRT-PCR on transcribed cDNA and normalized to expression of *GAPDH*. Average relative mRNA expression is shown as mean ± SEM (n = 5). (**C**) Expression of *Ctsg* and *serpinb3a/b/c* from IFN-γ–activated BMDMs infected with *M. tuberculosis* for 4, 24, and 72 hours, measured by qRT-PCR on transcribed cDNA relative to uninfected IFN-γ–activated BMDMs, with expression levels normalized to expression of *GAPDH*. Data are shown as mean ± SEM of 4 separate experiments. (**D**) Percentage of cell death of WT or *Serpinb3a*$^{-/-}$ BMDMs cultured in vitro, with or without IFN-γ–activation, measured as the percentage LDH activity in cell supernatants at 72 hours p.i. (MOI 2). Percentage LDH activity is shown as mean ± SD (n = 6). *M. tuberculosis* growth, evaluated by [3H] uracil incorporation at 72 hours p.i., is shown as mean cpm ± SD (n = 6). $^{**}P < 0.01$.

Methods

Mice. C57BL/6 mice were purchased from Charles River Laboratories, and *Nos2*$^{-/-}$ C57BL/6 and BALB/c mice (The Jackson Laboratory) were bred in our facilities. BALB/c *Serpinb3a*$^{-/-}$ mice were purchased from Charles River Laboratories. Infected mice were maintained at biosafety level 3, under specific pathogen–free conditions, and all animal experiments were approved by the local ethics committee of the German authorities (Landesamtes für Gesundheit und Soziales Berlin).

Infection with M. tuberculosis. The *M. tuberculosis* strain H37Rv (ATCC) was cultured in Middlebrook 7H9 broth (Difco) supplemented with 0.05% (v/v) Tween 80 and Middlebrook ADC Enrichment (BD) until mid-log phase (OD $_{600\ nm}$ 0.6–0.8). Bacteria were harvested, resuspended in PBS, and frozen at –80°C until use. For aerosol infection, mice received a dose of approximately 10^2 *M. tuberculsis* in the lung, using an inhalation exposure system (Glas-Col). For dermal infections, mice were anesthetized with i.p. administration of ketamine (50 mg/kg) and Rompun (5 mg/kg; Bayer), and 10^4 *M. tuberculosis* in a volume of 10 μl PBS was injected into the ear dermis.

In vivo cytokine blocking and AEBSF treatment. For cytokine blocking, dermal-infected *Nos2*$^{-/-}$ mice received 500 μg mAb purified from MP6-XT-22 (anti–TNF-α) or XMG1.2 (anti–IFN-γ) hybridomas (ATCC) i.p. in PBS on days 14 and 21 p.i. A control group of dermal-infected *Nos2*$^{-/-}$ mice were left untreated. To specifically inhibit serine proteases in vivo, IFN-γ–blocked dermal-infected *Nos2*$^{-/-}$ mice received 1 mg AEBSF (Enzo Life Sciences) i.p. in PBS twice weekly, from day 30 until day 60 p.i. A control group of IFN-γ–blocked dermal-infected *Nos2*$^{-/-}$ mice were left untreated.

Enumeration of CFUs. Mice were sacrificed at time points described, and organs were aseptically removed and homogenized in 1 ml PBS containing 0.05% Tween 80 (v/v). For CFU determination of the ear dermis, ears were removed, washed in 70% ethanol, and dried in air in a class II biosafety hood. Dorsal and ventral dermal layers were separated, cut into small pieces, and incubated in 1 mg/ml collagenase type VIII (Sigma-Aldrich) and 30 μg/ml DNase I (Roche) at 37°C for 30 minutes. Homogenates were then diluted in PBS containing 0.05% v/v Tween 80 and plated onto Middlebrook 7H11 agar plates supplemented with Middlebrook OADC Enrichment (Difco). CFUs were enumerated after 3 to 4 weeks of incubation at 37°C.

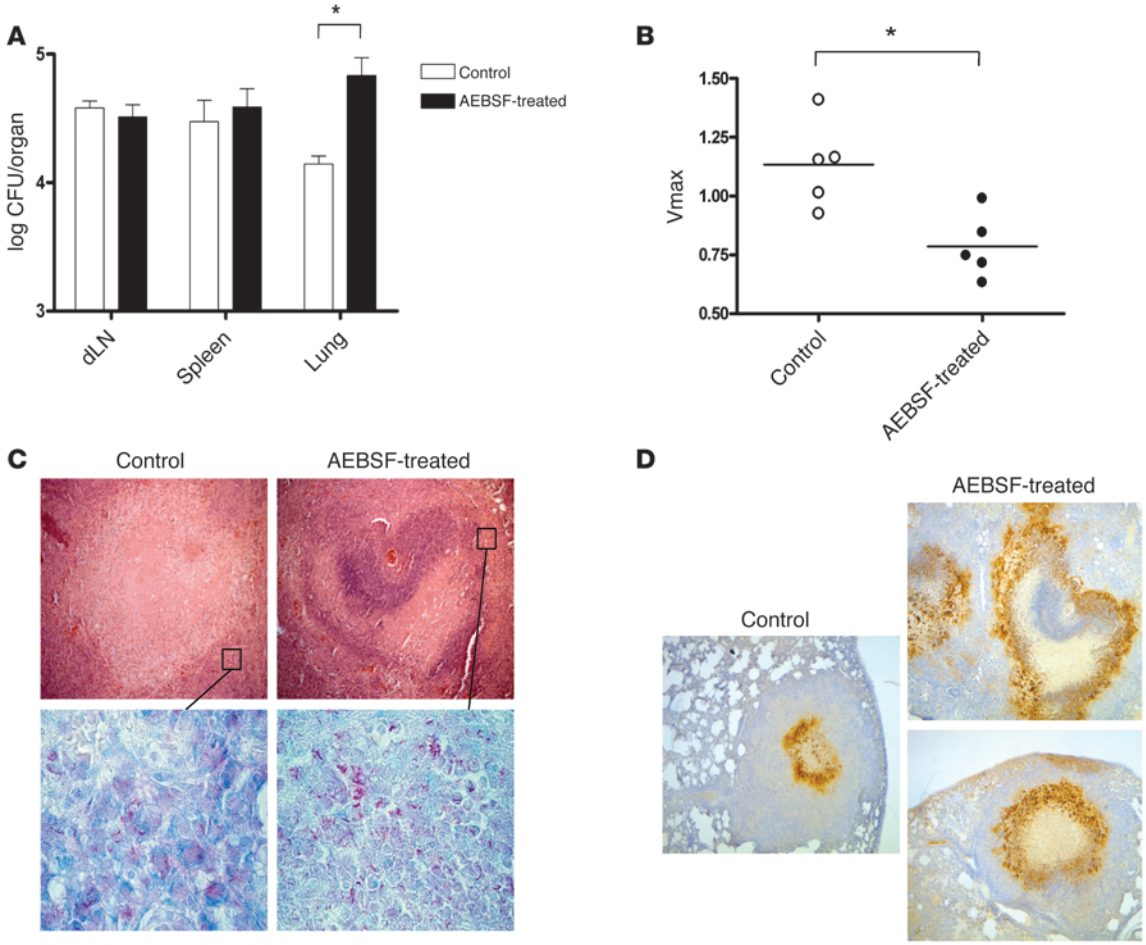

Figure 6
Serine protease activity in hypoxic regions of granulomas protects against tuberculosis. (**A**) The bacterial burden of tissue homogenates from dermal-infected IFN-γ–blocked *Nos2*$^{-/-}$ mice in dLN, spleen, and lung after twice weekly treatment with AEBSF. CFUs at day 56 p.i. are shown as mean ± SEM (n = 5). The control group did not receive AEBSF. (**B**) Vmax of chymotrypsin-like serine protease activity in lung lysates at day 56 p.i. from control and AEBSF-treated mice (n = 5). AEBSF treatment resulted in a significant reduction in Vmax in the lung but not complete inhibition of chymotrypsin-like serine protease activity. Horizontal lines indicate the mean Vmax. (**C**) H&E staining of lung granulomas with central necrosis from control and AEBSF-treated mice (original magnification, ×100) at day 56 p.i. revealed loss of granuloma structural integrity. Acid-fast *M. tuberculosis* was detected using a modified basic fuchsin stain in AEBSF-treated mice, which identified enhanced bacterial growth in regions encircling the necrotic zone demonstrated to be hypoxic, demonstrating elevated Ctsg and serpinb3a/b/c expression. Regions within the rectangles are shown at higher magnification (original magnification, ×1,000). (**D**) PIMO staining of granulomas in control mice and AEBSF-treated mice (original magnification, ×50), for which staining shows distortion of granuloma structure and extensive development of hypoxia in AEBSF-treated mice compared with control mice. *P < 0.05.

Histology. Formalin-fixed and paraffin-embedded tissue samples, taken from patients who underwent treatment for tuberculosis at the Charité Campus Benjamin Franklin, were retrieved from the archives of the Institute of Pathology, Charité Campus Benjamin Franklin. The use of human biopsies as anonymous samples was based on informed patient consent and approved by the ethics commission of Charité — Universitätsmedizin Berlin. At the time points described, mice were sacrificed and the lungs aseptically removed and fixed in PBS containing 4% w/v PFA for 24 hours at 4°C. Two- to three-μm thick sections of formalin-fixed, paraffin-embedded tissue were cut, deparaffinized, and subjected to H&E, Giemsa, and Ziehl Neelsen modified basic fuchsin stain for acid-fast bacteria (59) or immunostaining. For immunostaining, sections were subjected to a heat-induced epitope retrieval step. Slides were rinsed in cool running water, washed in Tris-buffered saline (pH 7.4), and incubated with primary antibodies against CD3 (N1580, Dako; 1:10), F4/80 (eBioscience; 1:50), Ctsg (I-19, Santa Cruz Biotechnology Inc.; 1:100), CTSG (19C3, Abcam; 1:100), serpinb3a/b/c (anti-serpinb3a clone 1-1, generated in this study [see below]; 1:100), MPO (A0398, Dako; 1:100), and CD68 (PG-M1, Dako; 1:50) for 30 minutes. For detection, biotinylated rabbit anti-rat, rabbit anti-goat (Dako), donkey anti-rabbit (Dianova), and goat anti–Armenian hamster (Dianova) secondary antibodies were used, followed by detection with the streptavidin-AP kit (K5005, Dako). Alkaline phosphatase was revealed by Fast Red as a chromogen. Negative controls were performed by omitting the primary antibody. Granulomas were quantified in H&E-stained sections of the whole left lobe of the lung. A minimum of 50 individual sections per mouse from each group (n = 5) were used to evaluate total granulomas per section. Caseous granulomas were defined as containing a pink central acellular necrotic region surrounded by granulomatous inflamma-

tory infiltrate. Granuloma hypoxia was evaluated on lung sections using the hypoxia marker PIMO Kit Hydroxyprobe-1 (Natural Pharmacia International), according to manufacturer's instructions. Twenty to fifty lung sections containing granulomas were evaluated for PIMO straining per mouse from each group (n = 5), with an analogous section subjected to H&E staining to confirm nonnecrotizing or caseous phenotype.

Development of anti-Serpinb3a mAb. Anti-mouse Serpinb3a mAb was developed by immunizing Armenian hamsters with purified His-tagged Serpinb3a fusion protein (48) (Cell Essentials). Spleen cell myeloma hybridomas secreting IgG recognizing GST-Serpinb3a fusion proteins were identified by ELISA and subcloned. Purified IgG from anti-Serpinb3a clone 1-1 detected GST-Serpinb3a and GST-Serpin3b, as evaluated by ELISA. Clone 1-1 recognized a single approximately 42-kDa molecular mass protein in lung extracts from WT BALB/c mice but not those from *Serpinb3a*$^{-/-}$ BALB/c mice using Western blot. Purified IgG clone 1-1 was detected using goat, anti–Armenian hamster secondary antibodies (Jackson ImmunoResearch Laboratories Inc.).

RNA isolation and qRT-PCR. For in vivo RNA isolation, lungs were aseptically removed from dermal-infected mice at day 28 p.i. and homogenized in TRIzol total RNA isolation reagent (Invitrogen). For in vitro RNA isolation from BMDMs, cells were harvested in TRIzol at the time points described. RNA was isolated from TRIzol via chloroform extraction and treatment with ethanol and dissolved in RNase-free water. RNA was analyzed for quality and quantified using a NanoDrop 1000 Spectrophotometer (Thermo Fischer Scientific). One μg RNA template was reverse-transcribed using SuperScript III Reverse Transcriptase (Invitrogen) and 10 ng cDNA was subjected to qRT-PCR using universal *serpinb3a/b/c* forward, CATTTGTTTGCTGAAGCCACTAC, and reverse, TCATGCCAGAGAAGTCAGCCTT, primers and *Ctsg* forward, TCCGCAGAACATCCGGAAT, and reverse, TTTTTTGCTGGCCTGAGGC, primers. Uptake of SYBR Green (Applied Biosystems) was measured using an ABI PRISM 7900 thermocycler (Applied Biosystems). CT values were normalized to those obtained for *GAPDH*, and $2^{-\Delta\Delta CT}$ was used to calculate change in relative mRNA expression between groups.

Intracellular cytokine staining. Mice were sacrificed, and cells were isolated from lungs of individual mice. Lungs were cut into small pieces and incubated in complete RPMI-10 medium (Invitrogen) supplemented with a 1 mg/ml blend of collagenase VIII and collagenase D (Roche) and 30 μg/ml DNase I for 30 minutes at 37°C in 5% CO_2. Lung homogenates were pressed through metal sieves, and cells were harvested by centrifugation through a percoll gradient. Red blood cells were lysed in ammonium chloride buffer, cells were washed with PBS containing 0.2% BSA, and 2×10^6 cells per well were added to 96-well tissue culture plates (Nunc). Cells were stimulated for 6 hours at 37°C in 5% CO_2 with 50 μg/ml PPD (Statens Serum Institut) and 10^{-4} M ESAT-$6_{61–80}$ (MTEQQWNFAGIEAAASAIQG) or incubated without protein/peptide stimulation. Cells were blocked after antigen stimulation with rat serum and αCD16/CD32 mAb, surface stained with αCD4-PacificBlue (RM4-5, BD Pharmingen) and αCD8-PerCP (53-6.7, BD Pharmingen) mAb, fixed with 2% PFA in PBS, permeabilized in saponin buffer, and stained with αIFN-γ–PE-Cy7 (XMG1.2, BD Pharmingen) and αTNF-α–FITC (MP6-XT-22, ATCC) mAb. Fifty thousand to one hundred thousand lymphocyte-gated $CD4^+$ T cells were acquired from each sample using a FACS Canto II (BD Pharmingen) and analyzed using BD Fascia software.

Competitive microarray analysis. Microarray experiments were performed as dual-color hybridizations. To compensate for dye-specific effects, a dye-reversal color-swap was applied. Total RNA was isolated using the TRIzol Reagent RNA preparation method (Invitrogen), using glycogen as carrier. Quality control and quantification of the total RNA amount was assessed using an Agilent 2100 Bioanalyzer (Agilent Technologies) and a NanoDrop 1000 Spectrophotometer (Kisker). RNA labeling was performed with the Low RNA Input Fluorescent Linear Amplification Kit (Agilent Technologies). In brief, mRNA was reverse-transcribed and amplified using an oligo-dT-T7-promotor primer (New England Biolabs), and resulting cRNA was labeled either with Cyanine 3-CTP or Cyanine 5-CTP (both from New England Biolabs). After precipitation, purification, and quantification, 1.25 μg of each labeled cRNA was fragmented and hybridized to whole mouse genome 44k microarrays, according to the supplier's protocol (Agilent Technologies). Scanning of microarrays was performed with 5-μm resolution, using a DNA microarray laser scanner (Agilent Technologies). Raw microarray image data were analyzed with the Image Analysis/Feature Extraction software G2567AA (version A.9.5.1, Agilent). The extracted MAGE-ML files were analyzed with the Rosetta Resolver Biosoftware, Build 6.1 (Rosetta Biosoftware). Ratio profiles comprising single hybridizations were combined in an error-weighted fashion to create ratio experiments. A 1.5-fold change expression cut-off for ratio experiments was applied together with anticorrelation of ratio profiles, rendering the microarray analysis highly significant (P > 0.01), robust, and reproducible. The data presented here have been deposited in NCBI's Gene Expression Omnibus (GEO; http://www.ncbi.nlm.nih.gov/geo/) and are accessible through GEO Series accession number GSE14826.

In vitro infection of BMDMs. BMDMs were prepared from femurs and tibias of BALB/c WT and *Serpinb3a*$^{-/-}$ mice by incubating bone marrow cells in Petri dishes containing L929 conditioned DMEM (Invitrogen) for 5–6 days. BMDMs were removed from plates and resuspended in complete RPMI-10. For preparation of RNA for qRT-PCR or whole cell lysates, 1×10^6 BMDMs per well were added to 12-well tissue culture plates (Nunc). For LDH activity or [3H] uracil incorporation assay, 4×10^4 BMDMs per well were added to 96-well plates. Cells were activated with 100 units/ml mouse recombinant IFN-γ (Active Bioscience) and where appropriate supplemented 10 μg/ml CTSG or human NE (Athens Research and Technology), 350 μM L-NMMA or D-LMMA (Axxora) and incubated for 16–24 hours at 37°C in 5% CO_2, before infection with *M. tuberculosis*. H37Rv was cultured in Middlebrook 7H9 broth (Difco) supplemented with 0.05% (v/v) Tween 80 and Middlebrook ADC Enrichment until early log phase ($OD_{600\,nm}$ 0.3–0.6). Bacteria were harvested, washed in warm PBS, and passaged gently 10 times through a 27-gauge needle. Cells were infected at MOI 2.

LDH activity assay. BMDM necrosis was estimated by LDH activity in culture supernatant, determined by Cytotoxicity Detection Kit (Roche). Supernatants were harvested from cultured BMDMs 72 hours p.i. with *M. tuberculosis* and centrifuged in 0.22-μm SPIN-X filter tubes. LDH activity in supernatants was normalized to that of uninfected activated BMDMs, and an LDH activity of 100% was calculated from complete chemical lysis of infected IFN-γ–activated BMDMs.

Protease activity assay. A portion of the left lobe of the lung was aseptically removed from mice, frozen in liquid N_2, and thawed by addition to 1 ml tissue lysis buffer (2 mM Tris, pH 7.2, 100 μM EDTA, 100 μM NaN_3, 50 mM NaCl, 0.1% Igepal). Tissue was homogenized and centrifuged at 6,708 *g*. Supernatants were then centrifuged in 0.22-μm SPIN-X filter tubes and snap frozen in liquid N_2. For the protease activity assay, suc-AAPF-pNA was dissolved in DMSO, and 100 μl of a 300 mM solution was added to an equivalent volume of 3 mg/ml lung lysate protein or pure CTSG in tissue lysis buffer. Cleavage of suc-AAPF-pNA was then followed by absorbance at 410 nm for 1 hour, with measurements taken every 2 minutes. Vmax of enzyme activity (r^2 > 0.99) was calculated using SoftMaxPro software (Molecular Devices). Using this assay for uninfected control mice, Vmax was less than 0 (n = 3).

[3H] uracil incorporation assay. Incorporation of [3H] uracil into bacterial RNA was used to evaluate levels of in vitro *M. tuberculosis* growth in BMDM cultures. One μCi [3H] uracil (Amersham) was added to BMDMs at 72 hours

p.i. with *M. tuberculosis*, and cells were incubated for a further 24 hours at 37°C in 5% CO_2. Cells were frozen at –80°C overnight, thawed, supplemented with 5% PFA, and incubated at room temperature for 2 hours. Samples were harvested onto Unifilter plates, scintillant was added, and cpm were determined using a TopCountNXT scintillation counter (Perkin Elmer).

Statistics. All statistical analyses were carried out using Prism 4 software (GraphPad). Individual comparisons were performed using a Mann Whitney test. Multiple group comparisons were performed using a Kruskal-Wallis test, followed by Dunn's multiple comparison test to compare individual groups.

Acknowledgments

Financial support for this work was received from the German Federal Ministry of Education and Research (Bundesministerium für Bildung und Forschung) Kompetenznetzwerk "PathoGenoMik-Plus" (to S.H.E. Kaufmann). Work by D.J. Askew and G.A. Silverman was supported by grants from the NIH (DK081422), and work by G.A. Silverman was supported by the Cystic Fibrosis Foundation.

Received for publication February 26, 2010, and accepted in revised form June 16, 2010.

Address correspondence to: Stephen T. Reece or Stefan H.E. Kaufmann, Department of Immunology, Max Planck Institute for Infection Biology, Charitéplatz 1, 10117 Berlin, Germany. Fax: 49.0.30.28460.505. Phone: 49.0.30.28460.552; E-mail: reece@mpiib-berlin.mpg.de (S. Reece). Phone: 49.0.30.28460.506; kaufmann@mpiib-berlin.mpg.de (S. Kaufmann).

Christoph Loddenkemper's present address is: Institute of Pathology, Technical University Munich, Munich, Germany.

1. Saunders BM, Britton WJ. Life and death in the granuloma: immunopathology of tuberculosis. *Immunol Cell Biol*. 2007;85(2):103–111.
2. Ulrichs T, Kaufmann SH. New insights into the function of granulomas in human tuberculosis. *J Pathol*. 2006;208(2):261–269.
3. Wallis RS, Broder MS, Wong JY, Hanson ME, Beenhouwer DO. Granulomatous infectious diseases associated with tumor necrosis factor antagonists. *Clin Infect Dis*. 2004;38(9):1261–1265.
4. Keane J, et al. Tuberculosis associated with infliximab, a tumor necrosis factor alpha-neutralizing agent. *N Engl J Med*. 2001;345(15):1098–1104.
5. Kaufmann SH, McMichael AJ. Annulling a dangerous liaison: vaccination strategies against AIDS and tuberculosis. *Nat Med*. 2005;11(4 suppl):S33–S44.
6. Kaplan G, et al. Mycobacterium tuberculosis growth at the cavity surface: a microenvironment with failed immunity. *Infect Immun*. 2003;71(12):7099–7108.
7. Loring WE, Vandiviere HM. The treated pulmonary lesion and its tubercle bacillus. I. Pathology and pathogenesis. *Am J Med Sci*. 1956;232(1):20–29.
8. Ghon A. *Der primäre Lungenherd bei der Tuberkulose der Kinder*. [The Primary Lung Lesion Of Infant Tuberculosis]. Berlin, Germany: Urban and Schwarzenberg; 1912.
9. Dannenberg AM. Pathogenesis of Human Pulmonary Tuberculosis. Washington DC, USA: ASM Press; 2006.
10. Boshoff HI, Barry CE 3rd. Tuberculosis - metabolism and respiration in the absence of growth. *Nat Rev Microbiol*. 2005;3(1):70–80.
11. Young DB, Perkins MD, Duncan K, Barry CE 3rd. Confronting the scientific obstacles to global control of tuberculosis. *J Clin Invest*. 2008;118(4):1255–1265.
12. North RJ, Jung YJ. Immunity to tuberculosis. *Annu Rev Immunol*. 2004;22:599–623.
13. Aly S, et al. Oxygen status of lung granulomas in Mycobacterium tuberculosis-infected mice. *J Pathol*. 2006;210(3):298–305.
14. Via LE, et al. Tuberculous granulomas are hypoxic in guinea pigs, rabbits, and nonhuman primates. *Infect Immun*. 2008;76(6):2333–2340.
15. Marcoval J, Servitje O, Moreno A, Jucgla A, Peyri J. Lupus vulgaris. Clinical, histopathologic, and bacteriologic study of 10 cases. *J Am Acad Dermatol*. 1992;26(3 pt 2):404–407.
16. Bravo FG, Gotuzzo E. Cutaneous tuberculosis. *Clin Dermatol*. 2007;25(2):173–180.
17. Chan J, Xing Y, Magliozzo RS, Bloom BR. Killing of virulent Mycobacterium tuberculosis by reactive nitrogen intermediates produced by activated murine macrophages. *J Exp Med*. 1992;175(4):1111–1122.
18. MacMicking JD, North RJ, LaCourse R, Mudgett JS, Shah SK, Nathan CF. Identification of nitric oxide synthase as a protective locus against tuberculosis. *Proc Natl Acad Sci U S A*. 1997;94(10):5243–5248.
19. Scanga CA, Mohan VP, Tanaka K, Alland D, Flynn JL, Chan J. The inducible nitric oxide synthase locus confers protection against aerogenic challenge of both clinical and laboratory strains of Mycobacterium tuberculosis in mice. *Infect Immun*. 2001;69(12):7711–7717.
20. Gonzalez-Juarrero M, Turner OC, Turner J, Marietta P, Brooks JV, Orme IM. Temporal and spatial arrangement of lymphocytes within lung granulomas induced by aerosol infection with Mycobacterium tuberculosis. *Infect Immun*. 2001;69(3):1722–1728.
21. Jung YJ, LaCourse R, Ryan L, North RJ. Virulent but not avirulent Mycobacterium tuberculosis can evade the growth inhibitory action of a T helper 1-dependent, nitric oxide Synthase 2-independent defense in mice. *J Exp Med*. 2002;196(7):991–998.
22. de Noronha A, Báfica A, Nogueira L, Barral A, Barral-Netto M. Lung granulomas from Mycobacterium tuberculosis/HIV-1 co-infected patients display decreased in situ TNF production. *Pathol Res Pract*. 2008;204(3):155–161.
23. Beisiegel M, et al. Combination of host susceptibility and virulence of Mycobacterium tuberculosis determines dual role of nitric oxide in the protection and control of inflammation. *J Infect Dis*. 2009;199(8):1222–1232.
24. Basaraba RJ. Experimental tuberculosis: the role of comparative pathology in the discovery of improved tuberculosis treatment strategies. *Tuberculosis (Edinb)*. 2008;88(suppl 1):S35–S47.
25. Yan BS, et al. Progression of pulmonary tuberculosis and efficiency of bacillus Calmette-Guerin vaccination are genetically controlled via a common sst1-mediated mechanism of innate immunity. *J Immunol*. 2007;179(10):6919–6932.
26. Pan H, et al. Ipr1 gene mediates innate immunity to tuberculosis. *Nature*. 2005;434(7034):767–772.
27. Lin PL, et al. Early events in Mycobacterium tuberculosis infection in cynomolgus macaques. *Infect Immun*. 2006;74(7):3790–3803.
28. Lin PL, et al. Quantitative comparison of active and latent tuberculosis in the cynomolgus macaque model. *Infect Immun*. 2009;77(10):4631–4642.
29. Raleigh JA, Chou SC, Bono EL, Thrall DE, Varia MA. Semiquantitative immunohistochemical analysis for hypoxia in human tumors. *Int J Radiat Oncol Biol Phys*. 2001;49(2):569–574.
30. Raleigh JA, Chou SC, Calkins-Adams DP, Ballenger CA, Novotny DB, Varia MA. A clinical study of hypoxia and metallothionein protein expression in squamous cell carcinomas. *Clin Cancer Res*. 2000;6(3):855–862.
31. Varia MA, et al. Pimonidazole: a novel hypoxia marker for complementary study of tumor hypoxia and cell proliferation in cervical carcinoma. *Gynecol Oncol*. 1998;71(2):270–277.
32. Reeves E, et al. Killing activity of neutrophils is mediated through activation of proteases by K+ flux. *Nature*. 2002;416(6878):291–297.
33. Belaaouaj A, et al. Mice lacking neutrophil elastase reveal impaired host defense against gram negative bacterial sepsis. *Nat Med*. 1998;4(5):615–618.
34. Pham CT. Neutrophil serine proteases: specific regulators of inflammation. *Nat Rev Immunol*. 2006;6(7):541–550.
35. Campbell EJ, Silverman EK, Campbell MA. Elastase and cathepsin G of human monocytes. Quantification of cellular content, release in response to stimuli, and heterogeneity in elastase-mediated proteolytic activity. *J Immunol*. 1989;143(9):2961–2968.
36. Kargi HA, Campbell EJ, Kuhn C 3rd. Elastase and cathepsin G of human monocytes: heterogeneity and subcellular localization to peroxidase-positive granules. *J Histochem Cytochem*. 1990;38(8):1179–1186.
37. Rivera-Marrero C, Stewart J, Shafer W, Roman J. The down-regulation of cathepsin G in THP-1 monocytes after infection with Mycobacterium tuberculosis is associated with increased intracellular survival of bacilli. *Infect Immun*. 2004; 72(10):5712–5721.
38. Caughey GH. A pulmonary perspective on GASPIDs: granule-associated serine peptidases of immune defense. *Curr Respir Med Rev*. 2006;2(39):263–277.
39. Robinson MA, Baumgardner JE, Good VP, Otto CM. Physiological and hypoxic O2 tensions rapidly regulate NO production by stimulated macrophages. *Am J Physiol Cell Physiol*. 2008; 294(4):C1079–C1087.
40. Nathan C. Microbiology. An antibiotic mimics immunity. *Science*. 2008;322(5906):1337–1338.
41. Benarafa C, Priebe GP, Remold-O'Donnell E. The neutrophil serine protease inhibitor serpinb1 preserves lung defense functions in Pseudomonas aeruginosa infection. *J Exp Med*. 2007;204(8):1901–1909.
42. Moraes TJ, Zurawska JH, Downey GP. Neutrophil granule contents in the pathogenesis of lung injury. *Curr Opin Hematol*. 2006;13(1):21–27.
43. Taggart CC, Greene CM, Carroll TP, O'Neill SJ, McElvaney NG. Elastolytic proteases: inflammation resolution and dysregulation in chronic infective lung disease. *Am J Respir Crit Care Med*. 2005;171(10):1070–1076.
44. Luke CJ, et al. An intracellular serpin regulates necrosis by inhibiting the induction and sequelae of lysosomal injury. *Cell*. 2007;130(6):1108–1119.
45. Silverman GA, et al. Human clade B serpins (ov-serpins) belong to a cohort of evolutionarily dispersed intracellular proteinase inhibitor clades that protect cells from promiscuous proteolysis. *Cell Mol Life Sci*. 2004;61(3):301–325.
46. Bartuski AJ, Kamachi Y, Schick C, Massa H, Trask BJ, Silverman GA. A murine ortholog of the human serpin SCCA2 maps to chromosome 1 and inhibits chymotrypsin-like serine proteinases. *Genomics*. 1998;54(2):297–306.

47. Al-Khunaizi M, et al. The serpin SQN-5 is a dual mechanistic-class inhibitor of serine and cysteine proteinases. *Biochemistry*. 2002;41(9):3189–3199.
48. Askew DJ, et al. The amplified mouse squamous cell carcinoma antigen gene locus contains a serpin (Serpinb3b) that inhibits both papain-like cysteine and trypsin-like serine proteinases. *Genomics*. 2004;84(1):166–175.
49. Buitrago-Rey R, Olarte J, Gomez-Marin JE. Evaluation of two inhibitors of invasion: LY311727 [3-(3-acetamide-1-benzyl-2-ethyl-indolyl-5-oxy)propane phosphonic acid] and AEBSF [4-(2-aminoethyl)-benzenesulphonyl fluoride] in acute murine toxoplasmosis. *J Antimicrob Chemother*. 2002;49(5):871–874.
50. Singh R, et al. PA-824 kills nonreplicating Mycobacterium tuberculosis by intracellular NO release. *Science*. 2008;322(5906):1392–1395.
51. Korkmaz B, Moreau T, Gauthier F. Neutrophil elastase, proteinase 3 and cathepsin G: physicochemical properties, activity and physiopathological functions. *Biochimie*. 2008;90(2):227–242.
52. Lehrer R, Ganz T. Antimicrobial polypeptides of human neutrophils. *Blood*. 1990;76(11):2169–2181.
53. Beisiegel M, et al. Combination of host susceptibility and Mycobacterium tuberculosis virulence define gene expression profile in the host. *Eur J Immunol*. 2009;39(12):3369–3384.
54. Grosset J. Mycobacterium tuberculosis in the extracellular compartment: an underestimated adversary. *Antimicrob Agents Chemother*. 2003;47(3):833–836.
55. Remold-O'Donnell E, Parent D. Downregulation of neutrophil CD43 by opsonized zymosan. *Blood*. 1995;85(2):337–342.
56. Andrews B, Bond K, Lehman J, Horn J, Dugan A, Gomez-Cambronero J. Direct inhibition of in vitro PLD activity by 4-(2-aminoethyl)-benzenesulfonyl fluoride. *Biochem Biophys Res Commun*. 2000;273(1):302–311.
57. Greco E, De Spirito M, Papi M, Fossati M, Auricchio G, Fraziano M. CpG oligodeoxynucleotides induce Ca2+-dependent phospholipase D activity leading to phagolysosome maturation and intracellular mycobacterial growth inhibition in monocytes. *Biochem Biophys Res Commun*. 2006;347(4):963–969.
58. Dannenberg AM Jr. Liquefaction and cavity formation in pulmonary TB: a simple method in rabbit skin to test inhibitors. *Tuberculosis (Edinb)*. 2009;89(4):243–247.
59. Ellis RC, Zabrowarny LA. Safer staining method for acid fast bacilli. *J Clin Pathol*. 1993;46(6):559–560.